Automatic Fault Detection of Photovoltaic Arrays by Convolutional Neural Networks During Aerial Infrared Thermography

3 authors:

Aline Kirsten Vidal de Oliveira
Universidade Federal de Santa Catarina
67 PUBLICATIONS   **496** CITATIONS

Mohammadreza Aghaei
191 PUBLICATIONS   **3,458** CITATIONS

Ricardo Rüther
Universidade Federal de Santa Catarina
368 PUBLICATIONS   **6,013** CITATIONS

AUTOMATIC FAULT DETECTION OF PHOTOVOLTAIC ARRAY BY CONVOLUTIONAL NEURAL NETWORKS DURING AERIAL INFRARED THERMOGRAPHY

Aline Kirsten Vidal de Oliveira[1], Mohammedreza Aghaei[2], Ricardo Rüther[1]
[1]Universidade Federal de Santa Catarina, Florianópolis–SC, 88056-000, Brazil
[2]University of Freiburg, Freiburg im Breisgau, 79085, Germany

ABSTRACT: Aerial Infrared Thermography (IRT) is a non-destructive and cost-effective method for detecting faults in large-scale photovoltaic (PV) power plants. However, the visual assessment of the images captured by aerial IRT, and the analysis of a large number of image frames is very time-consuming. This paper proposes a method for detecting and classifying faults on PV modules, through aerial IRT images, combining Digital Image Processing (DIP) and Convolutional Neural Networks (CNNs) algorithms. With the results obtained so far, the IR images acquired were successfully processed with DIP techniques to detect the faults of PV modules in the power plant that are used as samples for training the CNN. The developed neural network algorithm can detect faults on the aIRT images and classify them in three categories: disconnected substrings, hot spots, and disconnected strings. The results have demonstrated that the method is effective in detecting and classifying faults, and it is an important step for the full automation of aIRT inspection.
Keywords: System Performance, Monitoring, Aerial Infrared Thermography (aIRT), Automatic Fault Classification, Artificial Intelligence.

1 INTRODUCTION

Photovoltaics (PV) is currently the fastest growing segment of renewable energies worldwide. PV has become a competitive energy source and it has a great potential to expand, especially in the so-called Sunbelt countries. Brazil is one of these examples, reaching the benchmark of 2GW of installed PV capacity in early 2019 [1].

As the competitiveness of PV rises in the energy market, technology reliability is a major concern in the solar energy sector. Therefore, reliable and cost-effective methods of operation and maintenance (O&M) for PV power plants are of utmost importance to ensure safety, availability, and productivity of PV systems.

In recent years, various inspection and fault diagnosis methods have been developed. The most common methods include visual inspection, performance measurement (e.g. I-V curve tracing), electroluminescence (EL) and infrared thermography (IRT). Among these methods, IRT is one of the most popular and reliable fault diagnosis methods since it is a non-destructive method, requires minimum instrumentation, and can be carried out without interrupting the operation of PV plants. Furthermore, unlike electrical measurements, it provides information about the exact physical location of a defect in a fast and easy way [2].

In order to increase the accuracy and speed up the fault detection procedure for megawatt-scale PV power plants or PV systems with limited access like on rooftop or façades, IRT can be combined with Unmanned Aerial Vehicles (UAVs) [3]–[7]. Aerial inspection by UAV has the advantage of being a contactless, non-destructive and fast inspection method, which can be applied under real-time operating conditions. The use of this technique has become more widespread in recent years, mainly in multicrystalline silicon (m-Si) power plants.

However, the visual assessment of the images captured by aerial IRT, and the analysis of a large number of image frames is time-consuming. A solution to the problem is to automate the procedure of fault detection by combining aerial IRT with Digital Image Processing (DIP), as proposed by many authors [8]–[11].

A better way to approach the problem is to apply Artificial Neural Networks (ANNs) to categorize the different types of faults on PV modules. These intend to mimic the way the human brain performs a task of interest; therefore they are normally more assertive in complex tasks than traditional computation techniques [12]. Between the many different architectures of ANNs, Convolutional Neural Networks (CNNs) have demonstrated clear superiority in visual recognition tasks such as image classification and object detection. Their training is simple and they generate good results, even when the images are taken under different conditions [13].

This method was already explored for fault detection in [14], with high-quality results. However, the dataset created was based on human annotators, who segmented manually 3336 thermal images. Therefore, this procedure, in spite of being effective, is time-consuming for the replication of the technique using different cameras and different flight heights. A solution to the problem is to combine DIP techniques to create the required dataset in order to train the CNN.

This paper proposes a novel method for detecting and classifying faults on PV modules, through aerial IRT images by combining DIP and CNNs algorithms.

2 EXPERIMENTAL SETUP AND METHODS

The proposed method consists of four major steps: the acquisition of aIRT images, the application DIP techniques for image analytics, the creation of dataset and the classification/failure detection by the CNN. The steps are described in the following subsections.

2.1 Images Acquisition

For image acquisition, a UAV-based Aerial IRT-measurement system was developed using a DJI Phantom 3 Advanced model, as described in [6]. It was manipulated and equipped with a lightweight IRT camera (Thermoteknix MicroCAM 2) and a video transmission system. The IRT Camera has a spectral response range between 7 and 17 µm, and its resolution is 640 pixels. The

captured videos have a frame rate of 60 FPS. The dataset consists of frames of the videos that are recorded in grayscale and the intensity differences represent the temperature distribution on the modules.

The images were taken during the inspection of a 37 MWp PV power plant by UAV-based Aerial IRT-measurement system, covering a 97 hectares area in the Northeast of Brazil. The PV plant consists of more than one hundred N-S single-axis trackers. Each tracker controls the movement of more than one hundred m-Si 72 cells PV modules. The inspection was performed during the commissioning of the power plant, resulting in the detection of 86 modules with a disconnected substring, 8 disconnected strings, and two hot spots.

Inspection procedure and experimental setup were determined by IEC TS 62446-3. The flight altitude was set at 20 m in order to detect defects and failures on the PV modules and for reinforced Field of View (FoV) to cover at least three rows of PV arrays at the same time. The flight route was set trough GPS coordinates so the flight was steady with a constant velocity. The inspection duration was around 7 days.

2.2 DIP algorithm for the image analytics

The acquired images were captured in grayscale, which is clearer than coloured images. In grayscale, each pixel has an interval range between 0 and 255 (0 for black and 255 for white areas). Thus, the luminance of a pixel is usually described by one single byte, which corresponds to one of 256 levels. The DIP initiates with the pre-processing of the images. The first step of pre-processing is filtering to eliminate noise effects, despite causing blurred vision on the edge of the image. A Gaussian filter is chosen to decrease noise, highlighting the boundaries of PV modules and facilitating the segmentation part [8]. The contrast is adjusted in order to highlight the PV modules borders for the next steps. An additional fisheye reduction filter is applied in order to minimize the distortion of the camera.

For the detection of the areas of the image that correspond to the faults, the so-called segmentation step, the edges of the image should be highlighted. For that matter, a commonly used filter is the Laplacian operator, that calculates the gradient of the image. It highlights grey level discontinuities in an image and deemphasizes slowly varying grey level changes. It is useful in the process of borders detection, making the border of PV modules more visible. As the Laplacian operator is very sensitive to noise, the supra cited filtering step is important [15].

The next step is to transform the image into a binary image, using a threshold filter. The threshold selects the areas of the image that are clearer than a certain level, chosen after numerous trials. After this process, the result is a black-and-white mask, that has the lighter pixels of the original image as 1 and the darker as 0. The binary image also passes through a hole filling process, when possible holes are excluded, making the image clearer. Morphological operators as dilatation and opening are applied in order to filter the segments and obtain only the segments of interest. The final mask will have the pixels corresponding to the faults in the original image as 1 and the rest of the pixels as 0.

2.3 Creation of the dataset

Based on [16], the detected faults are classified into three categories: open strings, hot spots, and disconnected substrings.

In order to increase the number of images for the dataset, augmentation techniques are implemented. This process artificially enlarges the number of segments, aiming to improve the overall learning procedure and performance, by training the model with varied data. [17] Transformations are label preserving, and include rotations, dataset segments cropping and scaling, transposing and mirroring.

The dataset consists of infrared images with their corresponding ground-truth segmentation. It is prepared for two different tests. The first one uses a balanced quantity of samples for each category. It is limited by the number of frames available of the less common fault in the dataset (hot spot). The second one uses unbalanced categories, so it has a better chance to perform better on the detection of the fault category with more samples (disconnected substrings). In both datasets, 70% of the samples are used for training, 10% for validation and 20% for testing, as common in the literature. The same proportion is applied for each class.

2.4 Automatic Classification

For the automatic classification, the fine-tuning of a VGG-16 pre-trained model in Foreground Segmentation domain is employed using Keras and Tensor Flow [18]. The inputs of the algorithm are the aIRT images and the output, binary images with the segmentation of the faults. For avoiding overfitting, a dropout with a 50% rate is applied [19], [20].

To the evaluation of the performance of the algorithm, some metrics will be used as the precision, the efficiency and the sensibility of the obtained results.

3 RESULTS

After the acquisition procedure of the images in the PV power plant in the Northeast of Brazil, the frames of the collected videos were analysed and stored for the DIP. It was possible to obtain satisfactory results with simple computer vision techniques for segmenting the modules faults. It was necessary to develop various algorithms of DIP for different faults based on their specific shapes.

Fig. 1 illustrates some steps of the DIP after the pre-processing of the aIRT images. Fig. 1(a) shows the pre-processed initial image that contains a hot spot and a disconnected substring. Fig. 1(b) shows the image after a threshold filter. The blue areas are clearer than the chosen threshold, and are selected for the next steps. As the clearer pixels in the image represents the objects with higher temperature, the filter selected the faults on the modules and the ground. Fig. 1(c) shows how the segment (in yellow) turns out after a closing process, which eliminates holes in a segment that are smaller than a chosen kernel. Fig. 1(d) presents the resulting segment after the exclusion of all areas that touch the border of the images. This eliminates the ground of the images, so the remaining selected segment countains only the faults of the modules. Fig. 1(e) depicts the result of the DIP algorithm, after an opening of the segment to eliminate possible noise. The images demonstrate that it is possible to segment the faults on the images using DIP techniques. After the processing, the images were sorted and the ones with non-appropriate segments were excluded. This filtering is important in order to provide a good learning dataset for the CNN. Subsequently, the dataset was then prepared for the detection and classification of faults.
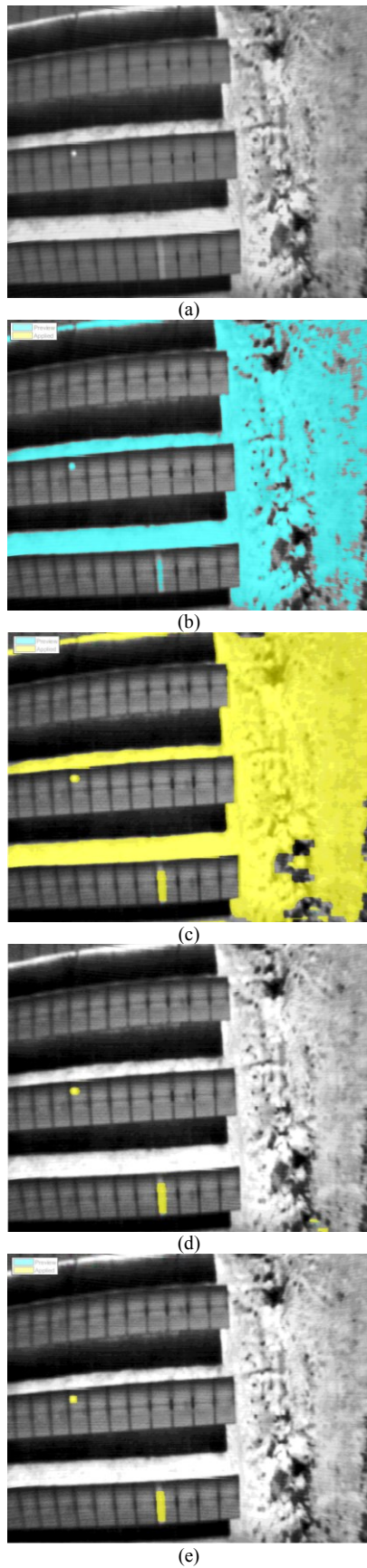
Figure 1: Steps of the segmentation of faults in an aIRT image. (a) Pre-processed image (b) Image after the threshold filter application. (c) Image after the closing of the segment (d) Image after the elimination of borders (e) Final image after the opening of the segment.

The automatic segmentation algorithm based on VGG-16 was successful to detect the determined faults, as shown in Fig. 2. The images show two examples of images used to validate the accuracy of the method.
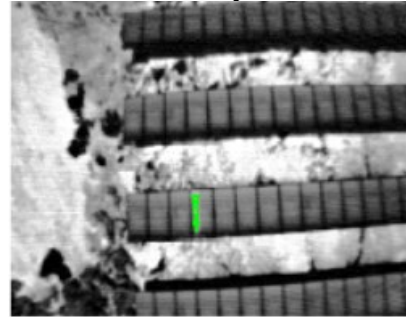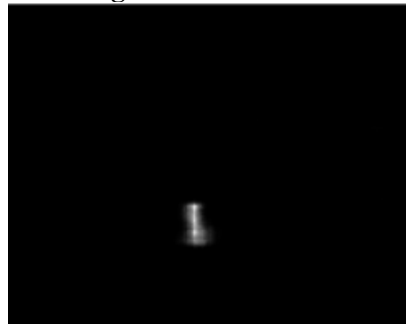
Test sample
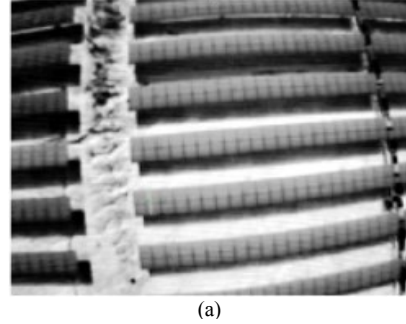
Segmentation result

Test sample

Segmentation result

Figure 2: Two examples of samples used as input of the segmentation algorithm for testing and the results obtained detecting PV modules with disconnected substrings. (a) IRT image of first example. (b) Output of the algorithm of first example. (c) IRT image of second example. (d) Output of the second example.

Fig. 2(a) and Fig. 2 (c) show the aIRT input image that the CNN receives for analysis. Fig. 2(b) and Fig. 2(d) show the segmentation given as an output. Both images contain PV modules with one disconnected substring, which were effectively detected by the CNN algorithm.

Good outcomes were also obtained on the detection of disconnected strings. Fig. 3 shows two examples of such faults that were successfully detected by the method. Fig. 3(a) and Fig. 3(c) present IRT images with disconnected strings and Fig. 3(b) and Fig. 3(d) present the outcome obtained with the algorithm. For the first case, an open string and a substring problem were correctly detected. For the second example, the four disconnected strings were detected (see Fig. 3(b)). However, the output presents a high level of noise, that is repeated in other images that contain many disconnected strings. In addition, a broken module, which can be identified by many hot spots on its IRT image, was not detected by the algorithm (see Fig. 3(d)). In general, the method was not successful in detecting hot spots, given the small dataset available for the training to detect this fault.

The algorithm could detect most of the faults on string and substring level on the samples, but it also identified many faults that did not exist. It generated more false-positive results (wrongly identified faults) than false negatives (faults that were not detected). This is an important achievement since false-positives can be removed with additional morphologic filters, in spite of false-negatives, that are more harmful.

The CNN could also detect faults that were not previously detected by the DIP algorithm (see Fig. 4). Fig. 4(a) shows the input image that had the expected response, given by the DIP techniques, shown in Fig. 4(b). This ground-truth presents the detection of four open strings. However, as seen in Fig. 4(c), the output of the CNN shows one module with a disconnected substring besides the four disconnected strings. This problem in the DIP algorithm happened because the module fault was subtle. Besides, the segmentation of the disconnected strings obtained with the CNN was more accurate than the ground-truth. This proves the superiority of the neural network to generalize and work on complex problems, on diverse image conditions.
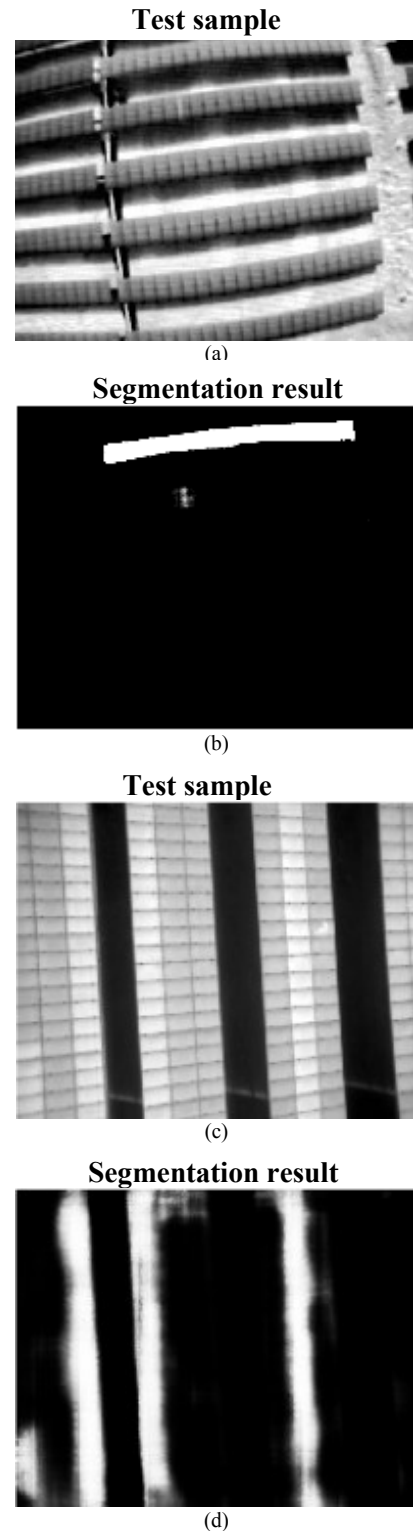
Test sample

(a)

Segmentation result

(b)

Test sample

(c)

Segmentation result

(d)

Figure 3: Two examples of samples used as input of the segmentation algorithm for testing and the results obtained detecting PV modules with disconnected substrings. (a) IRT image of first example. (b) Output of the algorithm of first example. (c) IRT image of second example. (d) Output of the second example.
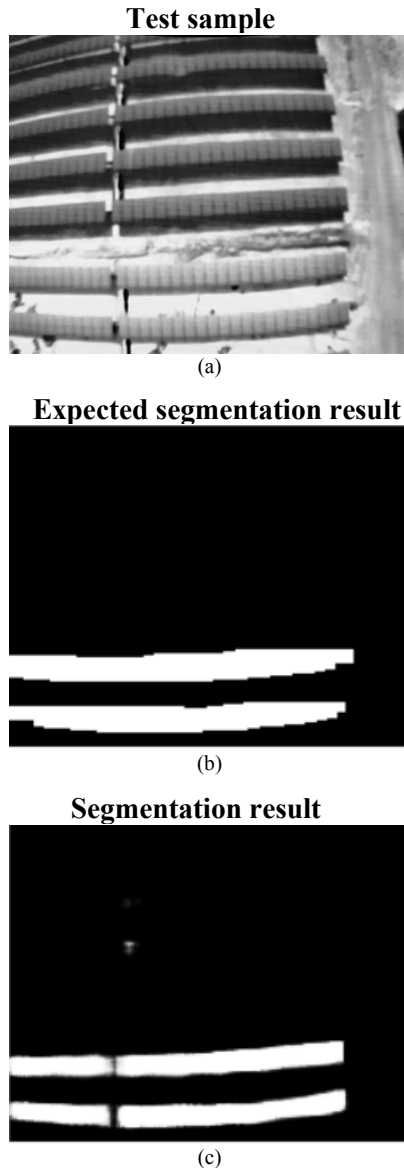
Test sample

(a)

Expected segmentation result

(b)

Segmentation result

(c)

Figure 4: Example of a sample used for testing of the CNN algorithm. (a) Original image, used as input for the model. (b) Target segmentation, obtained with DIP techniques. (c) Output obtained with the CNN algorithm.

4 CONCLUSIONS

This work has presented a novel method for automatic detection and classification of faults in PV power plants employing aIRT. The proposed method was successful in combining DIP techniques and CNNs in order to segment the PV modules faults correctly and classify them in three categories: disconnected substrings, hot spots, and disconnected strings. The algorithm was effective in detecting faults that were not detectable with the DIP techniques. However, it generated many false-positives, which had to be filtered.

The results have demonstrated that the method is very effective in detecting and classifying faults and it is an important step for the full automation of aIRT inspection.

6 REFERENCES

[1] ANEEL, "BIG - Banco de Informações de Geração," 2019. .

[2] C. Buerhop, D. Schlegel, M. Niess, C. Vodermayer, R. Weißmann, and C. J. Brabec, "Reliability of IR-imaging of PV-plants under operating conditions," *Sol. Energy Mater. Sol. Cells*, vol. 107, pp. 154–164, 2012.

[3] P. B. Quater, F. Grimaccia, S. Leva, M. Mussetta, and M. Aghaei, "Light Unmanned Aerial Vehicles (UAVs) for cooperative inspection of PV plants," *IEEE J. Photovoltaics*, vol. 4, no. 4, pp. 1107–1113, 2014.

[4] J. A. Tsanakas and P. N. Botsaris, "An infrared thermographic approach as a hot-spot detection tool for photovoltaic modules using image histogram and line profile analysis," *Int. J. Cond. Monit.*, vol. 2, no. 1, pp. 22–30, 2012.

[5] A. K. Vidal de Oliveira, D. Amstad, U. E. Madukanya, L. Rafael, M. Aghaei, and R. Rüther, "Aerial Infrared Thermography of a CdTe Utility-Scale PV Power Plant," in *46th IEEE PVSC*, 2019, pp. 1–6.

[6] A. Kirsten *et al.*, "Aerial Infrared Thermography of a Utility - S cale PV Power Plant A fter a Meteorological Tsunami in Brazil," in *WCPEC*, 2016, no. 20, pp. 1–3.

[7] M. Aghaei, P. B. Quater, F. Grimaccia, S. Leva, and M. Mussetta, "Unmanned Aerial Vehicles in Photovoltaic Systems Monitoring Applications," *29th Eur. Photovolt. Sol. Energy Conf. Exhib. (EU PVSEC 2014)*, no. 22-26 September, pp. 2734–2739, 2014.

[8] M. Aghaei, F. Grimaccia, C. A. Gonano, and S. Leva, "Innovative automated control system for PV fields inspection and remote control," *IEEE Trans. Ind. Electron.*, vol. 62, no. 11, pp. 7287–7296, 2015.

[9] F. B. John A. Tsanakas, Godefroy Vannier, Alexandre Plissonnier, Duy Long Ha, "Fault Diagnosis and Classification of Large-Scale Photovoltaic Plants through Aerial Orthophoto Thermal Mapping," in *31st European Photovoltaic Solar Energy Conference and Exhibition attached*, 2016, pp. 1783–1788.

[10] D. Kim, J. Youn, and C. Kim, "Automatic fault recognition of photovoltaic modules based on statistical analysis of UAV thermography," *Int. Arch. Photogramm. Remote Sens. Spat. Inf. Sci. - ISPRS Arch.*, vol. 42, no. 2W6, pp. 179–182, 2017.

[11] S. Rogotis, D. Ioannidis, a Tsolakis, D. Tzovaras, and S. Likothanassis, "Early defect diagnosis in installed PV modules exploiting spatio-temporal information from thermal images," *QIRT2014 Conférence*, 2014.

[12] R. C. Mayo and J. Leung, "Artificial intelligence and deep learning – Radiology's next frontier?," *Clin. Imaging*, vol. 49, no. July 2017, pp. 87–88, 2018.

[13] Q. Geng, Z. Zhou, and X. Cao, "Survey of recent progress in semantic image segmentation with CNNs," *Sci. China Inf. Sci.*, vol. 61, no. 5, pp. 1–18, 2018.

[14] R. Pierdicca, E. S. Malinverni, F. Piccinini, M. Paolanti, A. Felicetti, and P. Zingaretti, "Deep convolutional neural network for automatic detection of damaged photovoltaic cells," *Int. Arch. Photogramm. Remote Sens. Spat. Inf. Sci. - ISPRS Arch.*, vol. 42, no. 2, pp. 893–900, 2018.

[15] O. M. Filho and H. V. Neto, *Processamento Digital de Imagens*, vol. 21/03, no. 1. 1999.

[16] VATh, "Electrical Infrared Inspections ▪ Low Voltage," no. February, p. 17, 2016.

[17] A. Kamilaris and F. X. Prenafeta-Boldú, "Deep Learning in Agriculture: A Survey," *Comput. Electron. Agric.*, vol. 147, no. 1, pp. 70–90, 2018.

[18] F. O. R. L. Arge and C. I. Mage, "Very Deep Convolutional Networks for Large-Scale Image Recognition," in *ICLR 2015*, 2015, pp. 1–14.

[19] A. Krizhevsky, I. Sutskever, and G. E. Hinton, "ImageNet Classification with Deep Convolutional Neural Networks," *Adv. Neural Inf. Process. Syst.*, pp. 1–9, 2012.

[20] G. Hinton, "Dropout : A Simple Way to Prevent Neural Networks from Overfitting," vol. 15, pp. 1929–1958, 2014.